Electroencephalography and clinical Neurophysiology, 1984, 58: 481–497
Elsevier Scientific Publishers Ireland, Ltd.

92

Clinical Section

BIT-MAPPED COLOUR IMAGING OF THE POTENTIAL FIELDS OF PROPAGATED AND SEGMENTAL SUBCORTICAL COMPONENTS OF SOMATOSENSORY EVOKED POTENTIALS IN MAN [1]

JOHN E. DESMEDT and NGUYEN TRAN HUY

Brain Research Unit, University of Brussels, 115 Boulevard de Waterloo, Brussels 1000 (Belgium)

(Accepted for publication: August 28, 1984)

The diagnostic usefulness of somatosensory evoked potentials (SEPs) in clinical neurology is enhanced by precise delineation of the neural SEP generators. Electrode montages with a cephalic reference on the front (Matthews et al. 1974; Jones 1977; El Negamy and Sedgwick 1978; Small et al. 1980; Ganes and Nakstad 1984) involve inherent uncertainties whereas non-cephalic reference recordings (Cracco and Cracco 1976) can tell apart SEP components that are generated below or above the foramen magnum respectively (Desmedt and Cheron 1980, 1981a, b; Yamada et al. 1980, 1983; Anziska and Cracco 1981, 1983; Lueders et al. 1983; Mauguière et al. 1983a, b). Such components are confounded when using as reference a front electrode that records large positive far fields.

One factor influencing SEP field distributions is the axial orientation of neural generators (Lorente de Nó 1947; Desmedt et al. 1983; Kimura et al. 1983). In median nerve SEP the longitudinal axis of the spinal N11 generator offers a robust contrast to the horizontal axis of the N13 generator that was disclosed by non-invasive prevertebral recordings with oesophageal electrodes (Desmedt and Cheron 1981a; Desmedt 1984).

Current data should be extended by detailed spatial delineation of SEP fields and the present analysis is based on computerized colour-coded imaging of potential fields at the skin. After pioneering work by Walter and Shipton (1951), Rémond and Lesèvre (1965) and others, developments in high-speed computing and graphic display terminals afford novel imaging resources to extract the spatio-temporal information embedded in multichannel recordings (Estrin and Uzgalis 1969; Ragot and Rémond 1978; Duffy et al. 1978; Lehmann and Skrandies 1980; Buchsbaum et al. 1982; Desmedt and Bourguet 1985). The time history of SEP fields was visualized by spatio-temporal mapping or by animation effects through displaying series of frozen maps at, say, 1 msec intervals. The results documented several issues involving early SEP component.

Material and Methods

SEPs were recorded in 16 paid volunteers of 21–27 years (6 females) in good health, free from neurological disease and non-addicted to drugs. They gave informed consent and came back for repeat sessions. Selection was based on ability to relax and minimize muscle or eyeblink interference and on good yields in averaged SEPs. The awake subjects laid comfortably on a reclining chair in a sound-proofed, electrically shielded and air-conditioned room at 24°C, separate from the instrument control room.

The stimuli were square electrical pulses of 0.2 msec delivered by thin uncoated steel needles inserted 4 cm apart through the skin close to the left median or ulnar nerve at the wrist (cathode proximal). Intensities (3 times sensory threshold) eliciting a brisk twitch, but no pain, were monitored on

[1] This research has been supported by the Fonds de la Recherche Scientifique Médicale, Belgium.

Correspondence to: Prof. J.E. Desmedt, Brain Research Unit, 115 Boulevard de Waterloo, 1000 Brussels, Belgium, Tel. 322-538.08.44.

nixies hooked to a peak A/D detector chip in the primary of the stimulator output transformer. In other runs, stimuli were delivered through Medelec ring electrodes to fingers I–II–III, using a 1 msec delay for the thumb shock (Debecker and Desmedt 1964). Stimuli were usually triggered (delay circuit) between T and P waves of the electrocardiogram (ECG) to avoid ECG interference. Sometimes stimuli were triggered at 4–5/sec with on-line rejection (window trigger circuit) of samples with QRS peak of ECG. The arm skin temperature was 35°C.

Scalp and neck potentials were recorded with thin steel needles inserted into the skin. A flexible oesophageal probe terminated by 2 metal electrodes (Disa 13K63) was inserted through a nostril and adjusted under X-ray control for recording in front of vertebrae C5-C6 (Desmedt and Cheron 1981a). The non-cephalic reference was on the right-hand dorsum. Electrode impedance was below 3000 Ω. Homemade differential amplifiers (110 dB common mode rejection ratio at 1 kHz) of high input impedance (32 MΩ) with bandpass from 5 kHz to 1.6 Hz (Desmedt et al. 1974) fed a PDP 11-34 Digital Equipment computer (256 kbytes CPU-two RK — 06 discs). Bin width was 100 or 200 μsec. The overall gain was equal ±2% for the different channels. EEG was monitored on 16 Tektronix SC501 miniscopes. The software program rejected on-line any trial with amplifier overload or in which eyeblinks, eye movements or excess muscle potentials occurred. Details of method were given in Desmedt (1977). Data were plotted by computer graphics on paper. Components labels used P (positive) or N (negative) and modal peak latency in normal adults of standard body size (Donchin et al. 1977).

SEP fields mapping

Twenty-four electrodes were arranged in 3 horizontal planes around the neck: the upper plane was 4 cm below the inion and above the hyoid bone in front. The lower plane was at the C7 spinous process and above the sternal manubrium in front (Fig. 4). The middle plane was half way. The vertical separation of these horizontal planes was 40 or 45 mm depending on neck length. The mean neck circumference was 320 mm. The electrodes in each horizontal circle were equidistant and about 40 mm from each other (Fig. 5A).

For map computation the neck was considered as a perfect cylinder. The distribution of potential levels over the neck area was fitted by a quadratic surface with equation:

$$Vi = Ax_i^2 + By_i^2 + Cx_i^2 + Dx_iy_i + Ex_iz_i + Fy_iz_i + Gx_i + Hy_i + Iz_i + J$$

in which x_i, y_i and z_i were the coordinates of any chosen point on the neck area (Estrin and Uzgalis 1969). The number of recorded voltage functions exceeded the 10 parameters necessary to define the quadratic surface. The parameters were computed from a least-square fit using all 24 measured potential values. The residual differences between the polynomial value and the recorded potentials were made minimal in a least-square sense (Nielson 1956). For graphics imaging, the 3-dimensional surface of a half neck (e.g. between front and back midlines) was mapped onto a 2-dimensional plane by parallel projection, thus giving the visual impression of depth (Fig. 5A).

Alternately, spatio-temporal mapping of SEP changes over time used a linear array of electrodes around the neck (Fig. 5B) or along the midline (Fig. 6B). Areas with isopotential contours were computed by linear interpolation of potential differences between adjacent electrodes with respect to zero baseline (Rémond and Lesèvre 1965).

Bit-mapped colour images were drawn on paper with microprocessor-based Tektronix 4695 Color Graphics Copier which formed each pixel (picture element) of 1/30 in. by 4 rows of 4 dots of chosen colour combinations (black, cyan, magenta, yellow and white) according to computer commands for graphics imaging. Total graphic field width was 256 pixels.

Results

Fig. 1 presents SEPs recorded from the lower neck (B), oesophagus at the level of C5 (C) and midfrontal scalp (F) using non-cephalic reference. The P9 far field with identical onset latency throughout had a smaller voltage at lower neck (B). The N11 near field at lower neck (B) had an

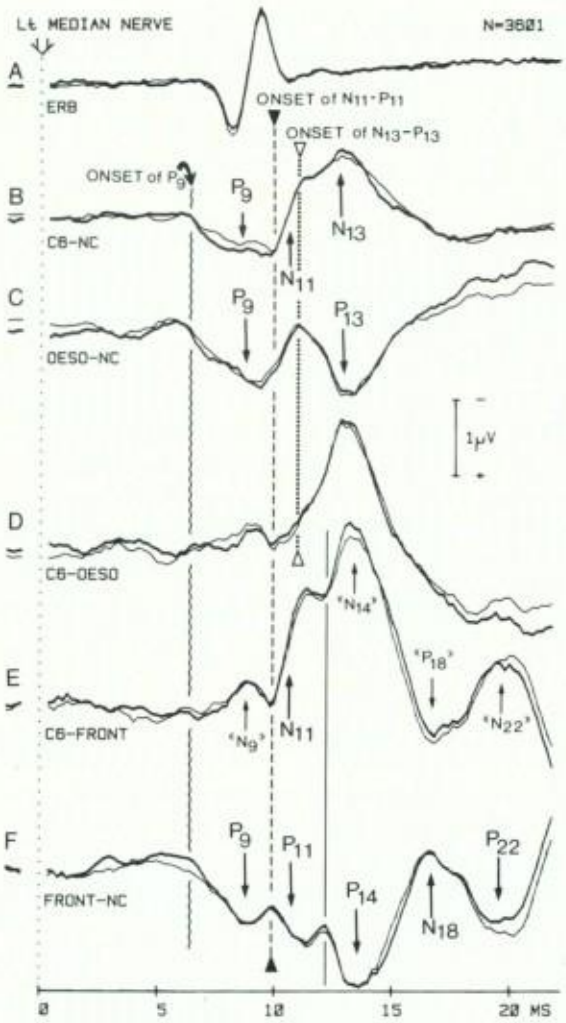

Fig. 1. SEPs to stimulation of the left median nerve at the wrist. The two traces superimposed represent a separate average of different runs to show consistency of wave form for the same electrode. Non-cephalic reference (NC) on the right-hand dorsum in A–C and F. A: recording from a fine needle inserted behind mid-clavicle at Erb's point. B: C6 spine at the posterior neck midline. C: oesophageal electrode in front of C6 vertebra. D: montage of C6 spine to oesophageal electrode. E: montage of C6 spine to front scalp. Components labelled 'N9,' 'N14,' 'P18' and 'N22' are contributed by the front reference and have inverted polarity. F: front scalp with non-cephalic reference. Negativity of the active electrode produces upward deflexion. The vertical wavy line identifies the onset of the P9 far field. The vertical interrupted line identifies onset of neck N11 or scalp P11. The vertical large dotted line identifies onset of N13-P13. Notice that N13 onset (C) occurs nearly 1 msec before P14 onset (F) and that P13 has a clearly longer duration than P14.

onset latency equal to that of the P11 scalp far field (F). The neck-to-front montage (E) enhanced the N11 negativity through algebraic addition with the P11 picked up by grid 2 of the amplifier, but did not alter N11 onset latency.

After P11, scalp recordings showed the P14 far field and this was added as a distinct 'N14' dome in the neck-front trace (E). The N18 and P22 responses of the front trace appeared with inverted polarity as 'P18' and 'N22' in this neck-front montage. The 'N9' in trace E was obviously formed through subtraction of the (larger) P9 at the front from the (smaller) P9 at lower neck. All such features were discussed in Desmedt and Cheron (1980, 1981b). The onset of negativity at Erb's point was later than the onset of P9 far field as the latter reflected the earlier arrival of the nerve volley about 80 mm distally to Erb's point (Desmedt et al. 1983).

New neck reference montage

The oesophageal trace (C) showed a P13 spinal response whose onset was better delineated than that of the concomitant N13 riding on N11 in the posterior neck trace (B). P13 was a phase reversal of N13, either of which reflecting an opposite side of the same spinal generator with horizontal axis (Desmedt and Cheron 1981a; Desmedt 1984). A useful new montage combined posterior neck C6 with an oesophageal reference (D) whereby N13 was boosted up.

Similar data were provided by the SEP to stimulation of the ulnar nerve at the wrist (Fig. 2). The oesophageal trace (C) showed a clear P13 whose summation with the neck N13 in oesophageal reference recording (D) resulted in a large negativity. The spinal N13-P13 response (B–C) was also distinct in latency and duration from the 'N14' added upon the neck trace in front scalp reference recording (E).

Latency and duration of components

The duration of the N13-P13 neck near field was significantly longer than that of the P14 scalp far field (Table I) (Desmedt and Cheron 1981b). Absolute SEP latencies varied in subjects with different arm length (Matthews et al. 1974; Abbruzzese et al. 1979; Small et al. 1980), yet the

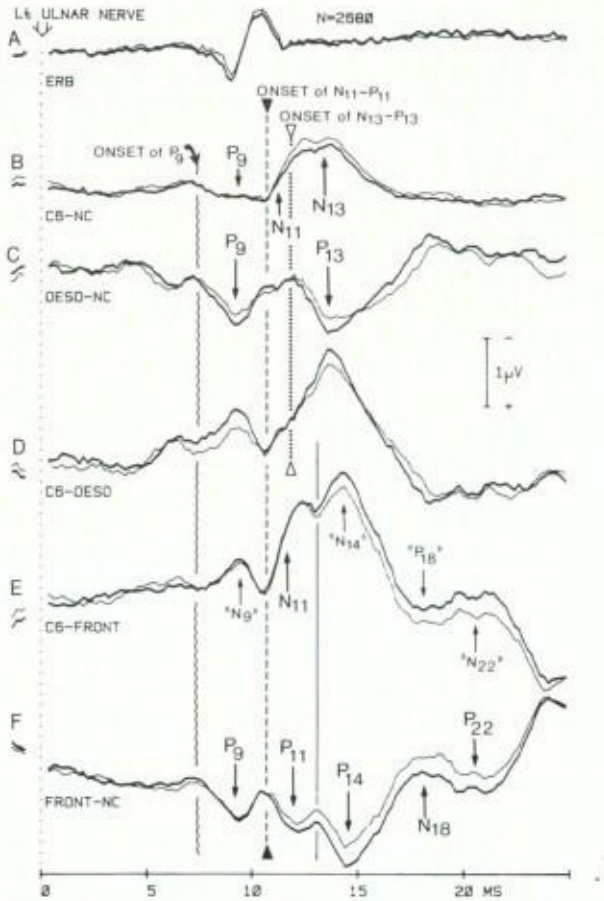

Fig. 2. Same presentation as in Fig. 1 for SEPs to stimulation of the left ulnar nerve at the wrist.

spinal P13 and scalp P14 peak latencies were significantly different (Table I).

Transit times were estimated from the onset of the neck N11 near field or scalp P11 far field which is thought to reflect the spinal entry time of the afferent volley (Desmedt and Cheron 1980, 1981b). The mean transit of 1.32 msec to the spinal P13 onset was shorter than the 2.03 msec to the scalp P14 onset and the difference was significant (Table I). Both values included one synaptic delay (in dorsal horn for P13 or in cuneate nucleus for P14), but the conduction distances and times were obviously different. The P14 onset latency included about 1.2 msec for conduction along the dorsal column from spinal entry to cuneate nucleus (Desmedt and Cheron, 1980, 1981b; Desmedt 1984). For the spinal P13, the conduction time was likely smaller along the (shorter) collateral branches from primary axons which coursed in spinal segments along (and penetrated) the mesial aspect of the dorsal horn.

SEP recorded at anterior neck

The phase reversal of N13 into P13 found in oesophageal recordings was also seen at the anterior neck (Fig. 3B) (Desmedt and Cheron 1981a, Fig. 8; Desmedt 1984). In posterior-to-anterior neck montages P13 was algebraically added to N13 (Fig. 3C). Similar features were seen for finger SEPs (E–F).

Electrodes at the anterior neck region recorded a triphasic spike (N10) reflecting a near-field pickup of the afferent volley in the proximal part of brachial plexus. This spike was much larger on the side of stimulation than contralaterally, and it was also larger at lower than at upper neck (Fig. 4A–C, F–H). It started with a positive approach wave that deepened the trough of the P9 far field. It was not surprising that this near-field root nega-

TABLE I

Data in 16 subjects comparing features of the spinal P13 recorded with the oesophageal probe in front of vertebra C5-C6 and of the scalp P14 far field.

	Spinal P13 Mean ± S.D.	Scalp P14 far field Mean ± S.D.	Difference and 95% confidence interval	*t* test by pairs
Peak latency (msec)	12.47 ± 0.76	13.27 ± 0.75	0.80 ± 0.25	$P < 0.001$
Duration (msec)	3.95 ± 0.88	2.61 ± 0.40	−1.34 ± 0.41	$P < 0.001$
Transit from onset of P11 to onset of (msec)	1.32 ± 0.23	2.03 ± 0.28	0.71 ± 0.18	$P < 0.001$

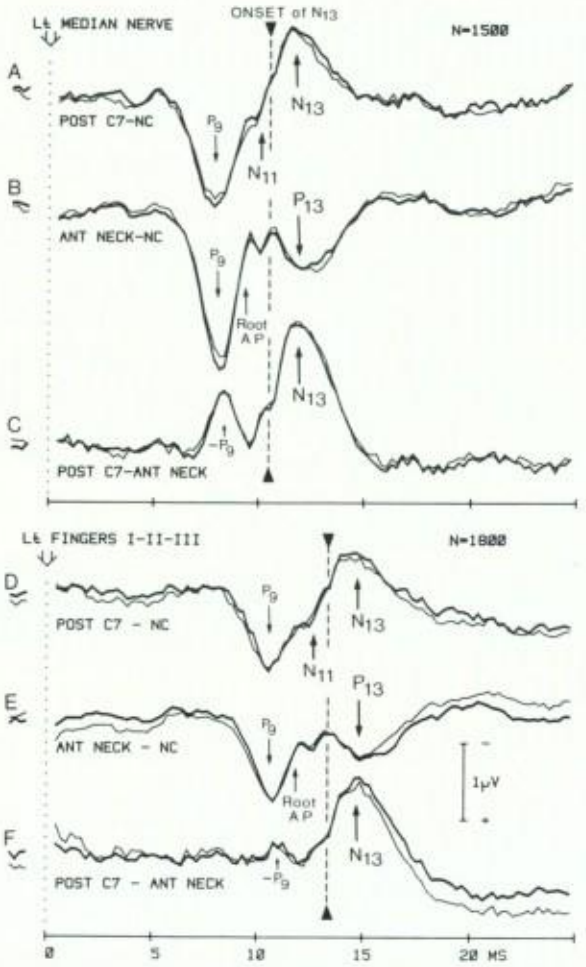

Fig. 3. SEPs to stimulation of the left median nerve (A–C) or left fingers I–II–III (D–F). Two averages of different runs are superimposed for each electrode montage. Non-cephalic (NC) reference on the right-hand dorsum. A and D: recording from C7 spine at posterior neck. B and E: skin electrode 4 cm to the right of the anterior midline at mid-neck. C and F: montage of C7 spine to anterior neck in which the '−P9' results from subtraction of the larger anterior P9. Vertical interrupted lines: N13-P13 onset.

tivity occurred later than the P9 *onset* which reflected the volley are more distal sites along the nerve (Desmedt et al. 1983, Fig. 5), nor that it started *before* the onset of N11 at posterior neck (Fig. 4D). This was expected if N11 was generated in dorsal column.

There may a problem of telling apart such near-field root spike from spinal components at electrodes on the side of nerve stimulation (Yamada et al. 1980). A cue may be the difference in wave forms at the lower posterior neck: the spinal N11 usually went negative from the bottom of the positive P9 trough (Figs. 4D and 9A), whereas the root spike had a clear triphasic profile starting with a large positivity (Fig. 4C, H).

For estimating the P13 onset, it was indeed more convenient to use anterior neck electrodes that were located about 4 cm to the right of the midline (thus contralaterally to the nerve stimulated) rather than on the midline or to the left (Fig. 3B, E). Spinal root spikes were much smaller in oesophageal records (Figs. 1C and 2C). For this reason, the data on P13 in Table I were estimated from oesophageal rather than from anterior neck traces.

Neck potential imaging

The 3-dimensional surface SEP fields over the right half-cylinder of the neck (contralateral to nerve stimulated) were displayed as a series of 2-dimensional frozen maps (Fig. 5A). The neck ipsilateral side was left out at this stage to avoid complexities from the large added root spike. Each electrode position was marked by a black pixel. The zero baseline ± 0.02 μV was in green. Voltage increments of 0.15 μV were represented by different hues of red for negative or blue for positive potential fields.

Each image in Fig. 5A is a frozen map at the latency indicated in msec after the left median nerve stimulus. Maps were presented at 0.5 msec intervals between 10.5 and 11.5 msec to show the progressive extension of the N11 negativity (red) from lower to upper neck. The N13 at posterior neck phase-reversed into P13 in front (peak 13 msec). The foci tended to be somewhat higher for P13 than for N13 and the boundary between them ran obliquely on the lower lateral side of the neck. The P9 far field was seen throughout the neck. Similar features related to P9, N11 and the N13-P13 phase reversal are displayed for another subject (Fig. 6A).

Spatio-temporal SEP imaging in a horizontal neck plane

Potential changes along time were mapped by a linear array of 8 electrodes placed on the mid-neck

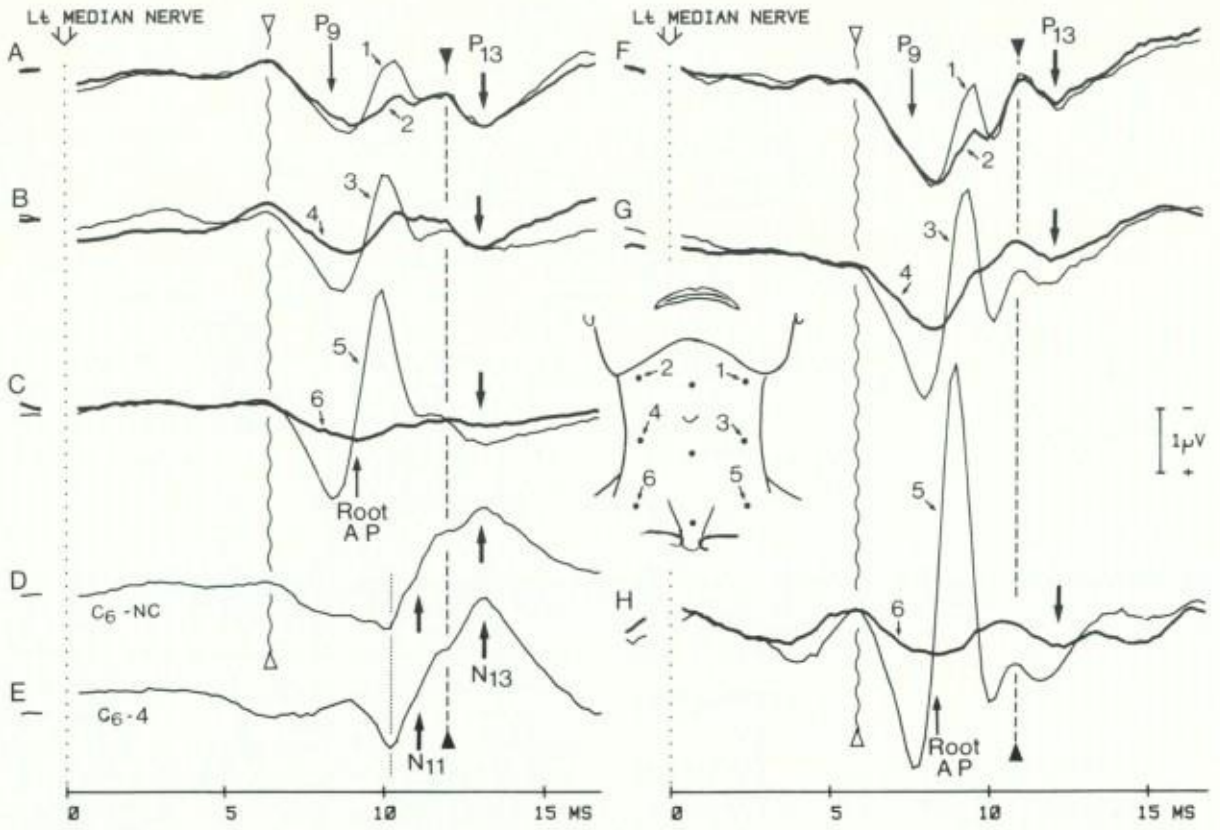

Fig. 4. SEPs to left median nerve stimulation at the wrist. Traces recorded 4 cm to the left or right of the anterior midline along the neck are superimposed. Non-cephalic reference (NC) on the right-hand dorsum. Electrodes labelled 1–6 are identified in figurine of anterior neck with head tilted backwards. A and F: upper neck plane of the electrode array. B and G: middle neck plane. C and H: lower neck plane. D: recording from the C6 spine at posterior neck midline. E: montage of C6 spine to the right anterior electrode (no. 4) at mid-neck. The vertical wavy line identifies the P9 onset and the vertical interrupted line the N13-P13 onset. Traces A–E were recorded in a male of 23 years. Traces F–H were recorded in a female of 22 years. An unusually large root spike was recorded at the left lower neck (H) in this skinny subject.

skin in a horizontal plane (Fig. 5B). Voltage values were fitted to a similar scale of equal discrete levels imaged by different hues of red (negative) or blue (positive). A synchronous P9 far field developed first and its voltage was larger in front. Then the root volley N10 appeared in red at the left anterior region where roots are running towards the spinal cord (see Fig. 4B, G), but not at the back. Thereafter an N11 appeared at the 3 posterior electrodes. The red negativity developed into the N13 peak while a concomitant blue-purple P13 positivity was seen in front. The space features of N13 and P13 fields were remarkably coherent, their peaks were synchronous and they dissipated in parallel.

Midline head SEP

Distinct SEP features were seen at lower or upper neck, or above the inion respectively (Fig. 7). The P9 far field extended from lower neck to nose. The N11 near field had a negative-going onset at the lower posterior neck (F–G), but was preceded at upper neck by a brief positivity (star) (D–E) (Desmedt and Cheron 1980; Lueders et al. 1983). This brief positive dip was interpreted as a volume-conducted positivity in front of the N11

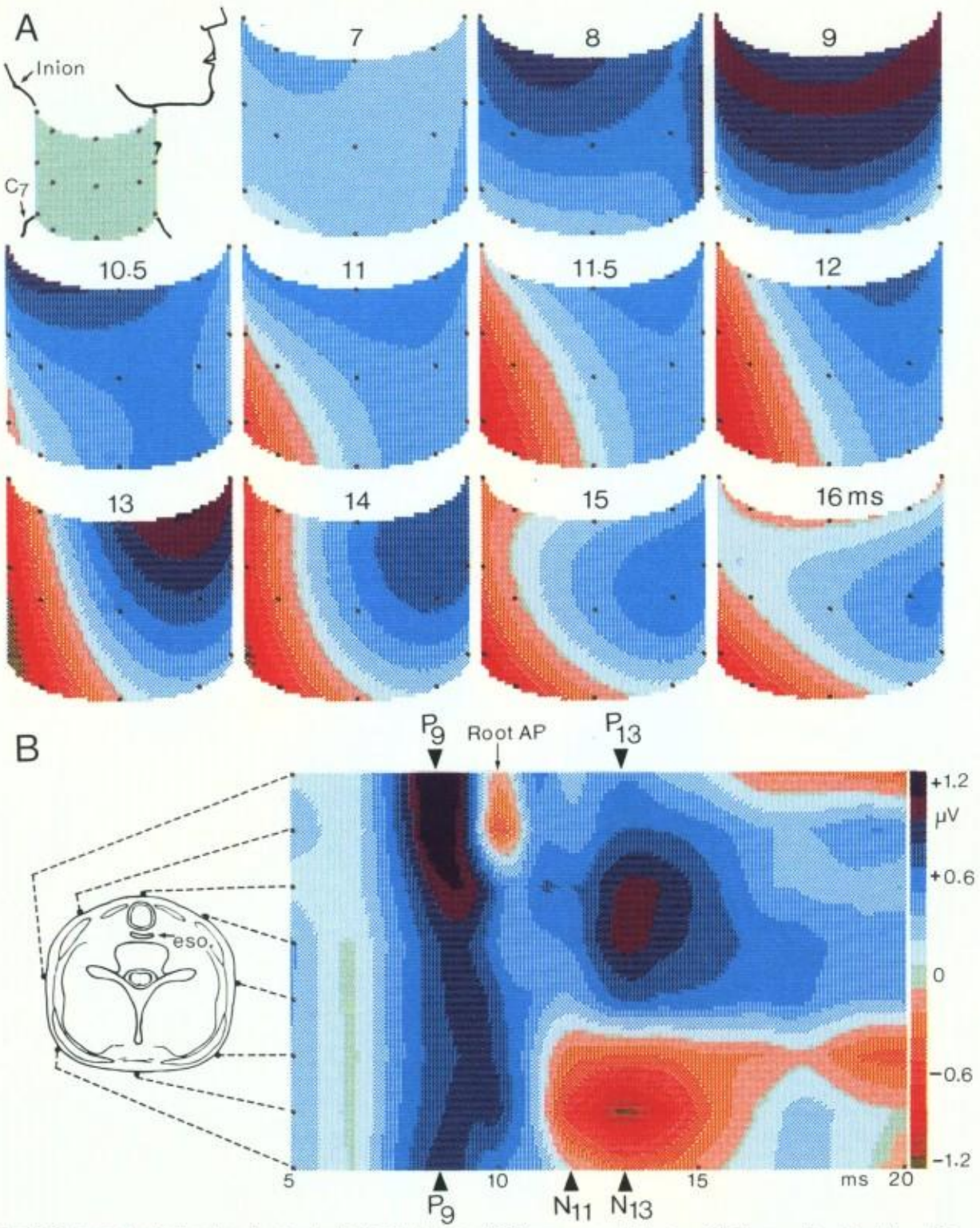

Fig. 5. Bit-mapped color imaging of neck potential fields. A: series of 11 frozen maps at latencies of 7–16 msec after stimulation of the left median nerve at the wrist. Each map images the right neck half-cylinder (see figurine). Electrode positions are indicated by black pixels. Voltage increments of 0.15 μV are represented by different hues in blue-purple for positive or red for negative. B: spatio-temporal map based on 8 electrodes in a horizontal plane at mid-neck. The time along the abscissa is from 5 to 20 msec after the left median nerve stimulus. Same calibration as in A.

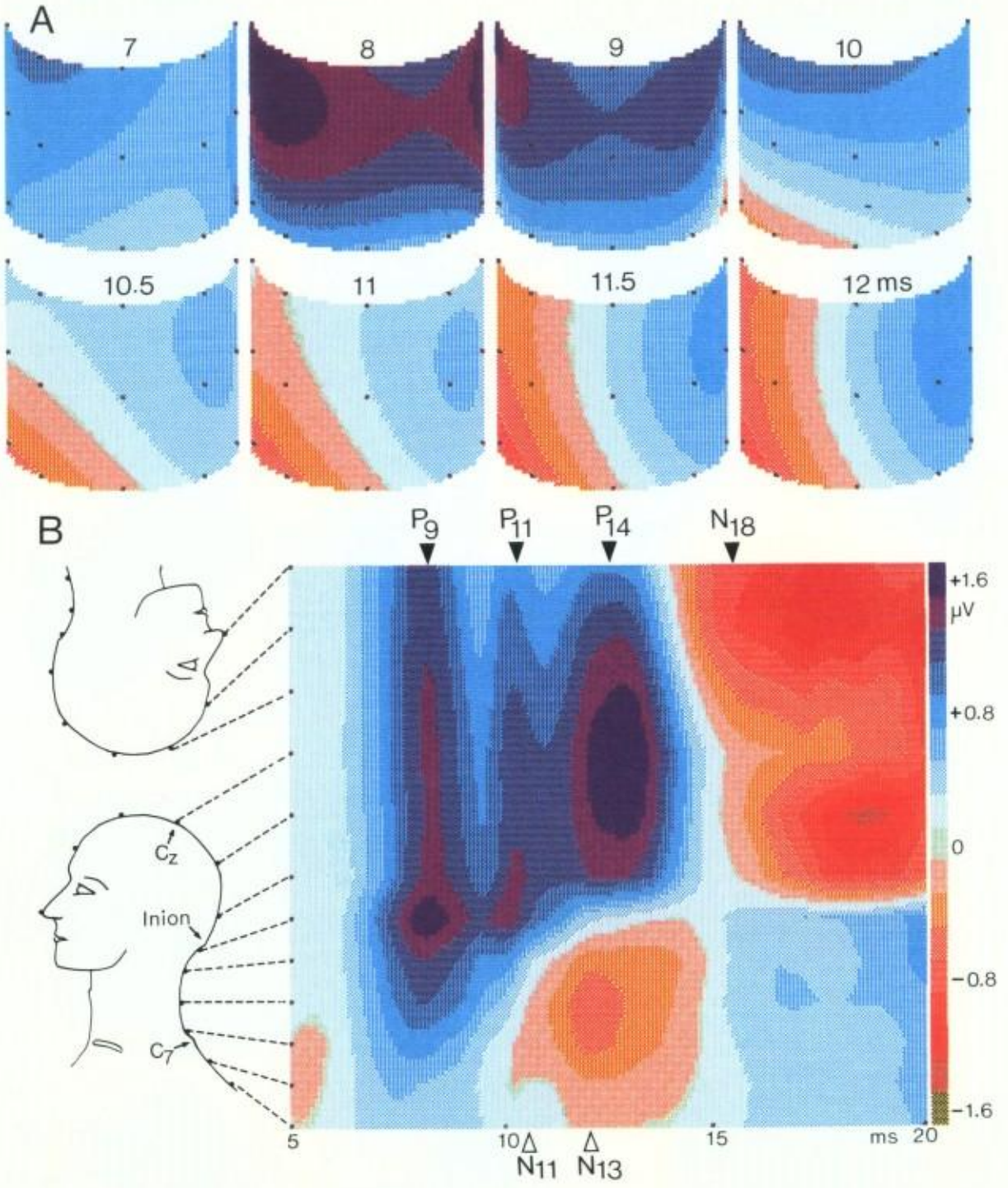

Fig. 6. A: series of 8 frozen maps at latencies of 7–12 msec after stimulation of the left median nerve at the wrist in another subject. B: spatio-temporal map based on 12 skin electrodes placed along the midline of the neck and scalp up to the tip of the nose (figurine). Voltage increments of 0.2 μV represented by different hues.

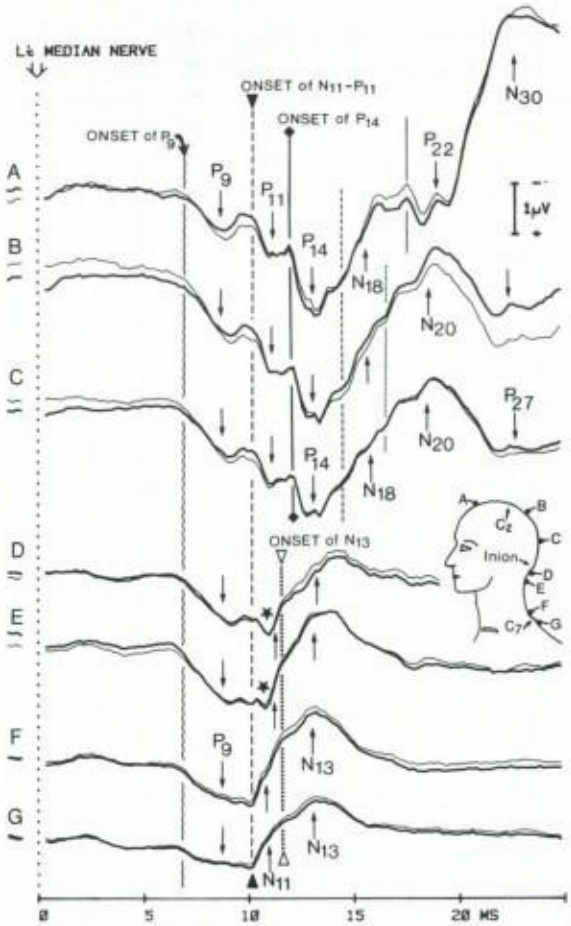

Fig. 7. SEPs to stimulation of the left median nerve at the wrist. Two separate averages of different runs are superimposed. Non-cephalic reference on the right-hand dorsum. All electrodes are along the midline. A: front (Fz) scalp. B–C: posterior scalp (figurine). D–E: upper posterior neck just below the inion. F–G: lower posterior neck above and below the C7 spine. The vertical wavy line identifies the P9 onset. The vertical interrupted line identifies onset of neck N11 or scalp P11. The vertical heavy dotted line identifies the onset of the spinal N13 which is not seen above the inion. The vertical black line identifies the P14 onset. Subsequent vertical markers identify the onset of the widespread N18, of the parietal N20 and of the prerolandic P22. Black star in D–E: positive dip in front of the N11 wave front of depolarization. N11 is not preceded by any positive dip at lower neck (F–G).

volley that was conducted up the dorsal column (Arezzo et al. 1979; Desmedt 1984). Thus, in neck-to-front montages, an active electrode at lower (rather than upper) neck had a more sharply featured and earlier onset that allowed more coherent algebraic addition to the P11 far field recorded by that reference at the frontal scalp (Fig. 8).

The spinal N13 rode upon N11 at the posterior neck and its onset in Fig. 7D–G was inferred through comparison with prevertebral P13 (see Fig. 1B–C). As N13-P13 had no latency shift along the neck (Desmedt and Cheron 1981a) while N11 had a later onset at upper neck, the N11 negativity crept underneath N13 at higher neck sites (Fig. 7). N13 was absent above the inion but the P14 far field with longer latency and shorter duration (Table I) was recorded. P14 was followed by a widespread N18, and by the cortical P22-N30 components at the prerolandic scalp. N20-P27 were

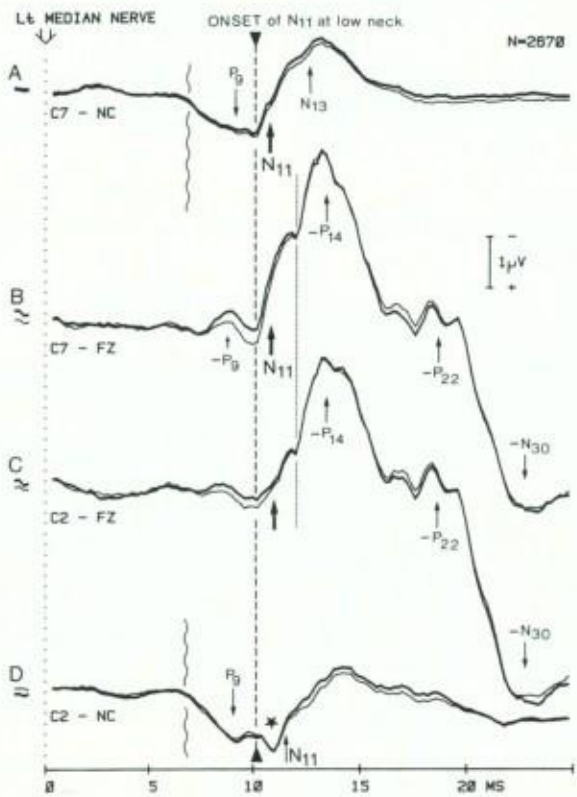

Fig. 8. Same experiment as in Fig. 7 to assess neck-to-front montages. A: lower posterior neck recorded with non-cephalic reference (same trace as in Fig. 7F). B: lower neck to Fz montage enhances the onset of N11 by subtraction of P11 far field, but a '−P14' is added on the neck profile, as well as other components. C: upper neck to Fz montage with N11 onset not so well delineated because the (same) P11 is subtracted from a later neck N11 that is preceded by the positive dip (see D). D: upper posterior neck recorded with non-cephalic reference (same trace as Fig. 7D).

poorly defined in Fig. 7B–C since the midline electrodes were at the margin of their (contralateral) field (Desmedt and Bourguet 1985).

Spatio-temporal imaging of head midline SEP

Potential fields imaged along time provided a striking display of far fields extending over the head. P9, P11 and P14 were each imaged as an elongated blue area whose axis was sharply vertical, indicating a stationary latency (Fig. 6B). The nose that had been used earlier as reference (Goff et al. 1962) was also involved. At the back, P14 failed to extend below the inion. P11 clearly encroached over the high neck during its initial part which corresponded to the positive approach seen in Fig. 7D–E. P9 extended further down to lower neck.

At 10–11 msec latency, the map showed over the neck a clearly oblique boundary between blue and red areas which provided yet another display of the latency shift of the onset of neck negativity N11 from lower to upper neck (Cracco and Cracco 1976; Desmedt and Cheron 1980; Desmedt 1984). By contrast the fairly vertical axis of the N13 focus was in line with the non-propagated generator of the spinal N13-P13 (Desmedt and Cheron 1981a, Fig. 5). Peak latency differed for the spinal N13 and the scalp P14 (Table I).

Significant SEP fields then occurred, not at the neck, but over the head with the extensive N18 negativity (Desmedt and Cheron 1981b; Mauguière et al. 1983b; Hashimoto 1984) with the superimposed parietal N20 and prerolandic N30. The prerolandic P22 only appeared as an area of lesser negativity in between.

Discussion

Bit-mapped colour imaging of evoked potential fields in the volume conductor of head and neck is a highly promising method for updating human brain electrophysiology. Accurate computerized displays can extract the pertinent spatio-temporal information embedded in multichannel electrical recordings. The creation of such imagery provides alternate displays whereby some current issues can be tested and discussions updated.

The present results substantiate key features of early SEP components to median nerve stimulation by identifying distinct spatio-temporal distributions for 5 major responses: the P9, P11 and P14 far fields, and the spinal N11 and N13 neck near fields. Some of these potentials like the neck N13 and the scalp P14 were confounded in neck-to-scalp (Fz) montages (Figs. 1E and 2E), but their differentiation through non-cephalic reference recordings has now been elaborated by field imaging methods.

The brachial plexus volley, P9 and N10

There is a wide consensus that P9 is a widespread far field reflecting the afferent volley in the brachial plexus (Cracco and Cracco 1976; Jones 1977; Kritchevsky and Wiederholt 1978; Chiappa et al. 1980; Desmedt and Cheron 1980; Yamada et al. 1980; Anziska and Cracco 1981; Lesser et al. 1981; Lueders et al. 1983). Comparison of P9 onset latency with direct recordings of the spike along the peripheral nerve indicated that the afferent volley starts generating P9 when it reaches a site under the lateral part of the clavicle (Desmedt and Cheron 1980). However, this site is not anatomically fixed: it can be shifted more proximally by about 8 cm (while P9 mean onset latency reduces by 1.15 msec) by merely placing the shoulder in a high position whereby the distal part of the brachial plexus acquires a more horizontal axis under the distal half of the clavicle (Desmedt et al. 1983). Such shifts of P9 *onset* latency did not affect P9 *peak* latency.

The total duration of P9, of about 3.5 msec (see Figs. 1B–F and 7), is definitely longer than the duration of other SEP far fields (for example, 1.5 msec for P11, Desmedt and Cheron 1981b) or of auditory brain-stem response peaks (Jewett and Williston 1971; Stockard and Sharbrough 1980). P9 duration must reflect the afferent volley during the time taken to travel from shoulder to spine. The length of brachial plexus and spinal roots concerned can be calculated as about: $71 \times 3.5 = 248$ mm. This is based on 71 m/sec as mean maximum conduction velocity of median nerve afferents (Desmedt and Cheron 1980) and on mean total duration of P9. When placing the arm in high-shoulder position, the initial 1.15 msec of this

duration are on average being removed from the P9 profile, thus leaving about 2.4 msec that include the P9 peak.

That the afferent volley should only start producing a P9 when it reaches a definite level along the nerve is most intriguing. Several factors can be mentioned. The tubular geometry of the arm no doubt limits the spread of extracellular potentials from the most distal part of the median nerve: thus the volley must apparently approach or enter the shoulder region to create recordable extracellular potentials in the head volume conductor. In addition, inhomogeneities and/or changes in geometry of the anatomical medium surrounding the nerve at that level may result in a more or less abrupt alteration of extracellular currents as the nerve volley reaches the brachial plexus, as indirectly hinted by the models described by Nakanishi (1982) and Kimura et al. (1983).

These factors may well determine at which site along the nerve the volley could possibly start being reflected in the far field. However, a third contingency, namely the axial orientation of the distal brachial plexus, appears to determine whether the P9 onset actually will be recorded when the volley reaches that level: with a horizontal axis, the volley must reach more proximal levels to begin generating P9 far field (Desmedt et al. 1983).

P9 does not require different labels at the head or neck (Yamada et al. 1983) and spatio-temporal maps image a single P9 field of stationary peak latency that extends from back to nose (Fig. 6B). P9 has a similar profile over the head and contralateral neck (Figs. 5 and 6) but, at the ipsilateral anterior neck, P9 is distorted by an N10 root volley that is recorded near field over the proximal brachial plexus and spinal roots (Fig. 4) (Yamada et al. 1980; Emerson et al. 1984). The P9 voltage appears maximum around the inion (Fig. 6B). In our dissections of cadavers, the proximal brachial plexus had a postero-superior oblique axis indeed targeted towards the back of the head.

The dorsal column propagated volley, N11 and P11

With non-cephalic reference, electrodes along the posterior neck record, after the P9 trough, an N11 whose onset latency increases from lower to upper neck (Fig. 7). Some viewed N11 as reflecting the root volley before entry into the spinal cord (Yamada et al. 1980, 1983; Shibasaki et al. 1982) or spinal canal (Lueders et al. 1983). However, the dorsal roots C6-C7 of median nerve reach the C5-C6 (not C1) vertebrae so that it is difficult to ascribe the N11 latency shift recorded at upper neck to a root volley. N11 rather reflects near-field recording from dorsal column (Desmedt and Cheron 1980; Anziska and Cracco 1981).

The cartoon of Fig. 9 depicts potential fields generated by an action potential volley conducted in an axon bundle of finite dimensions, like the dorsal column. Such a bundle is an 'open field system' (Lorente de Nó 1947) that generates extracellular potentials both at close range and at a distance (Klee and Rall 1977; Arezzo et al. 1979). As a volley is initiated at the caudal end of the bundle, the near-field electrode registers an ex-

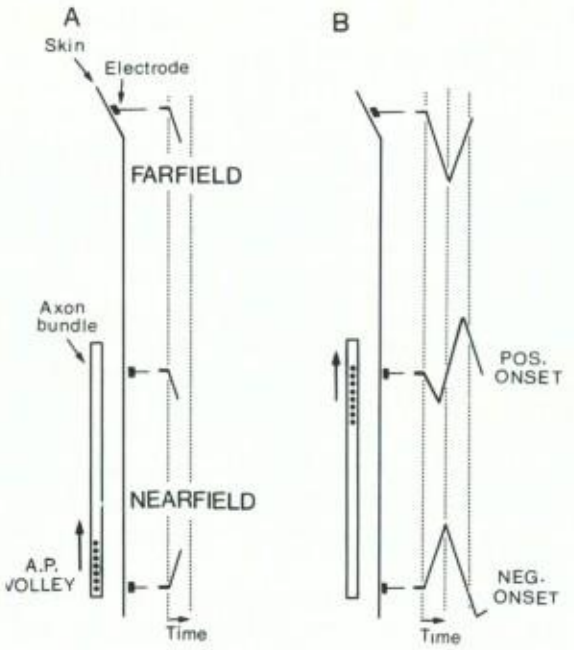

Fig. 9. Cartoon contrasting near-field recordings over a bundle of axons (such as the dorsal column) with finite dimensions and far-field recordings beyond the termination of the bundle. The part generating action potentials is pictured by heavy dots. The vertical dotted lines help identify time relationships. A: spike volley is initiated at the bottom end of axon bundle. B: the depolarization wave front has propagated to the level of the upper near-field electrode. The far-field electrode only records a monophasic positive wave.

tracellular negativity while distant electrodes higher up record an approach positivity. As the volley propagates to the upper near-field electrode it registers a negativity after the positive dip. Far-field electrodes located beyond pathway termination only register a monophasic positive deflexion (Arezzo et al. 1979; Desmedt 1984).

This model helps understand how the neck N11 and scalp P11 reflect the volley initiated in the dorsal column at the level of C6-C7 spinal segments (where median nerve afferents penetrate the spinal cord) and which propagates upwards along a caudo-rostral axis (Desmedt and Cheron 1980; Anziska and Cracco 1981). The volley propagates up to the termination of dorsal column axons in the cuneate nucleus which is located about 1 cm above foramen magnum and is thus not directly seen by an electrode over the C1 spine (Desmedt and Cheron 1980, Fig. 6).

With non-cephalic reference recording, N11 appears as a conducted negative front whose onset latency shifts on average by 0.94 msec from low to high neck in normal adults (Desmedt and Cheron 1981a). At the upper neck, an approach positivity precedes the wave front of the ascending depolarization (Fig. 7D–E). That N11 is a 'near-field' potential generated at close range with respect to the posterior neck electrodes (as in Fig. 9) is evidenced by the fact that changes of the electrode position along the axis of the dorsal column conductor indeed affect the N11 onset latency. Bony structures of the spinal canal (Lueders et al. 1983) do not appear to prevent recording this propagated negativity. By contrast, all electrodes located beyond the pathway termination record a positive P11 that shows a stable latency regardless of electrode positions in the far field of the head.

Spatio-temporal maps indeed image a P11 with stationary latency extending from nose to upper neck where it meets the N11 negativity (Fig. 6B). The oblique boundary between the red and blue areas at the neck images upward propagation of the N11 volley. Onset latencies are identical for the P11 (blue) dip over the head and for N11 (red) at *lower* neck. Latencies cannot be measured for the N11 peak that is buried underneath N13.

We take exception to Emerson et al. (1984) statement that subcortical generators would be reflected in scalp negativities rather than positive far fields as this contradicts classical volume conductor theory (Lorente de Nò 1947; Klee and Rall 1977; Arezzo et al. 1979; Desmedt 1984). The peak of their 'N10' (between P9 and P11) is what we call the P11 onset and the peak of their 'N12' (between P11 and P14) is our P14 onset. The issue is mainly semantic and the respective data concur if labels are properly exchanged. Emerson et al.'s argument that 'N10' and 'N12' may exceed the preceding baseline is weak because their records were differentiated by restricted bandpass (30 Hz highpass filter). With wide bandpass, the second negative-going limb of the P9 and P11 far fields remains below baseline (Figs. 1F, 2F and 7A–C) (see Cracco and Cracco 1976; Kritchevsky and Wiederholt 1978; Desmedt and Cheron 1980, 1981a, b; Yamada et al. 1980).

The dorsal horn segmental generator, N13 and the spinal P13

Non-cephalic reference recording from posterior neck shows that the N11 negative front is superimposed by a second negativity N13 which phase-reverses into a positive P13 at oesophageal sites in front of the spinal cord (Figs. 1B–C and 2B–C) (Desmedt and Cheron 1981a). An enhanced display of N13 is achieved in a neck-to-oesophagus montage (Figs. 1D and 2D).

Skin recordings at anterior neck also show the P13 phase reversal (Fig. 3) (Desmedt 1984). It is not surprising that such traces do not disclose a well-formed N11 which is thought to be generated in dorsal columns at the back of the spinal cord. On the other hand the anterior neck traces, especially on the side ipsilateral to the limb stimulated, include a triphasic spike (N10) representing the proximal brachial plexus volley (Fig. 4). N10 distorts oesophageal recordings to a lesser extent (Figs. 1C and 2C).

Topographical analyses are essential to identify the generators of SEP components peaking around 13 msec. With oesophageal recordings, the longitudinal extent of the spinal P13 potential field was analyzed along the oesophagus lumen at levels between the C1 and D3 vertebrae: P13 was found to be maximum between the C4 and D1 spinal cord levels and to sharply decrease in voltage

above C3 or below D1 (Desmedt and Cheron 1981a). That the oesophageal P13 onset latency did not change along the cord was also an important finding because the corresponding N13 at the posterior neck appears as a mere notch on the negative slope of N11-N13 and its onset is difficult to estimate reliably (Figs. 1B, 2B, 3A–B, 4D and 7D–G).

SEP field imaging allowed a complete survey of the neck volume conductor. For clarity, we emphasized the right half-cylinder of the neck from anterior to posterior midlines. N13 (red) appeared maximum over the lower half of the posterior neck while the concomitant P13 (blue) was maximum over the middle part of the anterior neck (Figs. 5A and 6A). The somewhat oblique boundary between the two was on the lateral side. The transition between the N11 and N13 negativities cannot be readily identified in these maps. Spatio-temporal mapping in a horizontal plane shows the remarkable similarity in peak latency and duration of the two components: this is crucial evidence for the hypothesis that prevertebral P13 is indeed a phase reversal of posterior neck N13, both sharing the same generator with horizontal axial orientation (Fig. 5B). Spatio-temporal maps confirm that the spinal N13-P13 are not volume-conducted more rostrally (Fig. 6B) and have distinct latency and duration than the scalp P14 far field (Table I).

Both oesophageal recordings and field mapping over the neck substantiate the segmental nature of the N13-P13 generator for which a dorsal horn location was suggested (Desmedt and Cheron 1981a; Desmedt 1984). After spinal entry, the large fibres of the dorsal roots bifurcate in the dorsal column into an ascending branch (reaching the cuneate nucleus) and a shorter descending branch. Collaterals of either branches penetrate into the mediodorsal aspect of the dorsal horn and form a dense plexus in the nucleus proprius (Cajal 1909; Sprague and Hong 1964; Rethelyi and Szentágothai 1973) which corresponds to cytoarchitectonic layers IV and V (Rexed 1954). The density of such collaterals is highest near root level (for median nerve afferents: C6-C7). From autopsy findings in patients with brachial plexus lesions (Dejérine and Thomas 1896) collaterals appear to be given off about 2 segments above and 2 segments below root entry in man. This fits well with our data of oesophageal recordings (Desmedt and Cheron 1981a) and field imaging (Fig. 6B).

N13 is the human equivalent of the first negative component of the cord dorsum potential of cat or monkey (Gasser and Graham 1933; Bernhard 1953; Lindblom and Ottoson 1953) which is evoked by lowest-threshold cutaneous A$\alpha\beta$ afferents (Beall et al. 1977; Willis and Coggeshall 1978). Intraspinal mapping with microelectrodes locate its maximum negativity in layers IV and V of the dorsal horn where many interneurones are postsynaptically activated by cutaneous input (Coombs et al. 1956; Wall 1967; Beall et al. 1977). The posterior negativity phase-reverses into a positivity in the ventral part of the spinal cord. Intraspinal recordings in cat or monkey show that the first negative wave of the cord dorsum potential follows a focal brief spike (in afferent axons) after a synaptic delay of 0.6 msec (Bernhard 1953) or 0.8 msec (Coombs et al. 1956; Beall et al. 1977). The duration of the negative wave is 4 msec (Bernhard 1953), 5 msec (Coombs et al. 1956) or 8.2 msec (Beall et al. 1977). These data are compatible with measures of the human P13 (oesophageal recording) features: mean duration of 3.95 msec and mean onset latency of 1.32 msec after spinal entry (Table I).

This robust set of data indicates that the posterior neck N13 reflects one side of the horizontal segmental generator in layers IV–V of the dorsal horn over the C4-D1 spinal segments while the oesophageal or anterior neck P13 reflects the opposite side of the same generator. N13-P13 have coherent space and time features which are compatible with a genuine phase-reversal. They are elicited, after one synaptic delay, in dorsal horn interneurones and represent postsynaptic excitatory potentials (Coombs et al. 1956) whose duration is significantly longer than that of the P11 or P14 far fields which reflect fibre tract volleys (Table I). The longitudinal axis of the (propagated) N11 generator contrasts with the horizontal axis of the N13-P13 segmental generator which produces no far field and, in particular, has no relation to the scalp P13-P14 far field.

The scalp P14

We lump under this label what is sometimes called the scalp P13-P14 (Table II) on the ground that P13 was absent or doubtful in as many of 44% of young adults (Desmedt and Cheron 1981b). We do not deny that more than one generator might be involved in this complex. From its mean onset latency 2.03 msec after spinal entry or P11 onset (Table I) P14 is unlikely to be generated in the spinal cord and it is not recorded below the inion (Fig. 6B). SEPs involve the dorsal column-lemniscal system (Halliday and Wakefield 1963; Noel and Desmedt 1975) and the dorsal column volley arrives at the level of C1 after a mean latency of 0.94 msec (Desmedt and Cheron 1981a) from which the arrival time at the cuneate nucleus can be estimated at about 1.2 msec. By adding to the latter figure the synaptic delay in the cuneate (roughly set at 0.6 or 0.8 msec), one gets rather close to the recorded onset latency of P14 at 2.03 msec after P11 onset (Table I).

The P14 duration is compatible with its being a far field reflecting the volley propagated in a subcortical fibre tract. Patients data indicate that P14 is lost after a high spinal hemisection (Mauguière et al. 1983a) but preserved after a thalamic lesion interrupting the somatosensory pathway completely (Nakanishi et al. 1978; Chiappa et al. 1980; Mauguière et al. 1983b). This evidence is compatible with P14 being generated in the longitudinally orientated medial lemniscus. Spatio-temporal imaging emphasizes the widespread scalp distribution and stationary latency of P14.

Practical considerations

Current clinical uses of SEPs would be assisted if a robust pathophysiological basis could be offered and if practical electrode montages and consistent component labels were widely agreed upon. Table II reviews labels used in recent publications. It would seem that standard labels for SEP components (rather than labels with different latencies as measured in particular cases) would facilitate discussions (Donchin et al. 1977). Anyway it may be useful to point out that the N11 and N13 spinal components are called 'N10' and 'N12' by Lueders et al. (1983), and that the 'N18' of Pratt et al. (1979), Lueders et al. (1983) and Yamada et al. (1983) is the contralateral parietal N20, but not the widespread N18 (or N16 of Hashimoto 1984) which persists after a thalamic lesion (Mauguière et al. 1983b).

Issues about montages may not be resolved so rapidly. Current evidence from several groups clearly differentiates spinal SEP components (N11, N13) from those generated above foramen magnum (P14). Therefore spinal or brain-stem lesions may not be readily identified for practical purposes by montages with cephalic reference in which these distinct generators are confounded. Peak latencies of neck-to-front montages do not relate to any spinal component, but to the P14 peak (seen as an 'N14') which reflects activity close to thalamus (Figs. 1E, 2E and 8). This may call for a reassessment of what is in fact being measured in current estimates of central conduction (Desmedt 1971; Hume and Cant 1978, 1981; Symon et al.

TABLE II

Labels of early SEP components used in recent publications. Most recordings considered use a wide bandpass (about 1–3000 Hz) and non-cephalic reference recording for far-field and neck SEPs. P9, P11 and P14 are the usual scalp far fields. N11 and N13 are the neck SEP components. N18 is the widespread negativity while N20 is the negative response recorded over the parietal scalp contralateral to the median nerve stimulated. The fact that this focal N20 is sometimes called N18 may result in misunderstandings. P27 is the contralateral parietal positive component.

Desmedt and Cheron 1981b	P9	N11	P11	N13	P14	N18	N20	P27
Mauguière et al. 1983b	P9	N11	P11	N13	P14	N18	N20	P27
Anziska and Cracco 1981, 1983	P9	N11	P11	N13	P13-P14	N18	N20	P23
Chiappa and Ropper 1982	–	N11	–	N13 (Fz ref)	P13	–	N19	P22
Lueders et al. 1983	P8	N10	P11	N12	P13	–	N18	P20
Yamada et al. 1983	P9	N11	P11	N13	P13-P14	–	N18	P23
Hashimoto 1984	P9		P11		P13-P14	N16	N20	P22
Pratt et al. 1979	P10	–	–	N13	P13-P14	–	N18	P22

1979; Chiappa and Ropper 1982).

The neck-to-front montage has one advantage though, namely to boost up the N11 negative front which facilitates the estimation of N11 *onset*. This is not distorted since the added scalp P11 is related to the same spinal generator as N11. The new montage of posterior to anterior neck may also be useful because it ensures a good signal-to-noise ratio while achieving a consistent algebraic addition of spinal potentials (N13 and P13) produced by the same segmental generator.

Summary

Early somatosensory evoked potentials (SEPs) to median or ulnar nerve stimulation were recorded with non-cephalic reference from neck, oesophagus and scalp in normal young adults. Transit times and durations were estimated for different components. SEP fields were mapped with up to 24 skin electrodes around the neck or along the midline neck and scalp, and projected onto a 2-dimensional plane for bit-mapped colour imaging. The posterior neck N11 is a near-field potential propagated caudorostrally in the dorsal column, associated with a positive P11 far field beyond termination of the cuneate bundle. A true phase reversal of the posterior neck N13 into an anterior neck P13 is substantiated, identifying a segmental generator with horizontal axis in dorsal horn. The N13-P13 represents postsynaptic excitatory potentials in interneurones of layers IV–V of the dorsal horn. It is not reflected in any scalp far field. The duration and onset latency of N13-P13 are in line with this interpretation. A new montage of posterior-to-anterior neck can enhance this component without introducing extraneous potentials. The P14 far field does not extend below the inion and presents distinct features. Neck-to-front scalp montages confound the SEP components generated in the spinal cord and above the foramen magnum respectively, but may serve to estimate N11 onset latency.

Résumé

Imagerie colorée des champs de potentiel des composantes sous-corticales propagées et non-propagées des potentiels évoqués somesthésiques chez l'homme

Les composantes précoces du potentiel évoqué somesthésique (PES) à la stimulation du nerf médian ou cubital ont été dérivées (référence non céphalique) au niveau du cou, de l'oesophage et du cuir chevelu chez de jeunes adultes normaux. Les temps de transit et les durées ont été mesurés pour diverses composantes. Les champs de potentiel ont été cartographiés autour du cou et le long de la ligne médiane avec jusqu'à 24 électrodes et projetés sur un plan bidimensionnel pour l'imagerie digitale en couleur. Le N11 de la nuque est un potentiel de champ proche propagé caudo-rostralement dans le cordon postérieur. Un potentiel de champ lointain P11 est produit concomitamment dans la tête au-delà de la terminaison du cordon postérieur. Les données confirment une réelle opposition de phase entre le N13 à la nuque et le P13 à la face antérieure du cou, indiquant un générateur horizontal dans la corne dorsale. Le N13-P13 représente des potentiels postsynaptiques excitateurs dans les interneurones de la couche IV–V de la corne dorsale. Il n'a pas d'équivalent dans le champ lointain. La durée et la latence initiale de N13-P13 sont en accord avec cette interprétation. Un nouveau montage référant la face postérieure du cou à sa face antérieure renforce ce potentiel sans introduire de composantes parasites. Le potentiel de champ lointain P14 ne s'étend pas en-dessous de l'inion et il présente des propriétés différentes. Les dérivations de la nuque avec référence front confondent les composantes produites respectivement par la moelle et au-dessus du trou occipital mais elles peuvent être utiles pour mesurer la latence initiale de N11.

References

Abbruzzese, M., Favale, E., Leandri, M. and Ratto, S. Electrophysiological assessment of the central lemniscal pathway in man. Experientia (Basel), 1979, 35: 775–776.

Anziska, B. and Cracco, R.Q. Short latency SEPs to median nerve stimulation: comparison of recording methods and

origin of components. Electroenceph. clin. Neurophysiol., 1981, 52: 531–539.

Anziska, B. and Cracco, R.Q. Short-latency somatosensory evoked potentials to median nerve stimulation in patients with diffuse neurologic disease. Neurology (Minneap.), 1983, 33: 989–993.

Arezzo, J., Legatt, A.D. and Vaughan, H.G. Topography and intracranial sources of somatosensory evoked potentials in the monkey. I. Early components. Electroenceph. clin. Neurophysiol., 1979, 46: 155–172.

Beall, J.E., Applebaum, A.E., Foreman, R.D. and Willis, W.D. Spinal cord potentials evoked by cutaneous afferents in the monkey. J. Neurophysiol., 1977, 40: 199–211.

Bernhard, C.G. The spinal cord potentials in leads from the cord dorsum in relation to the peripheral source of afferent stimulation. Acta physiol. scand., 1953, 29 (Suppl. 106): 1–29.

Buchsbaum, M.S., Rigal, F., Coppola, R., Cappelletti, J., King, C. and Johnson, J. A new system for gray-level surface distribution maps of electrical activity. Electroenceph. clin. Neurophysiol., 1982, 53: 237–242.

Cajal, S. Ramôn y. Histologie du Système Nerveux de l'Homme et des Vertébrés. Maloine, Paris, 1909.

Chiappa, K.H. and Ropper, A.H. Evoked potentials in clinical medicine. New Engl. J. Med., 1982, 306: 1205–1211.

Chiappa, K.H., Choi, S.K. and Young, R.R. Short-latency somatosensory evoked potentials following median nerve stimulation in patients with neurological lesions. In: J.E. Desmedt (Ed.), Clinical Uses of Cerebral, Brainstem and Spinal Somatosensory Evoked Potentials. Progr. clin. Neurophysiol., Vol. 7. Karger, Basel, 1980: 264–281.

Coombs, J.S., Curtis, D.R. and Landgren, S. Spinal cord potentials generated by impulses in muscle and cutaneous afferent fibres. J. Neurophysiol., 1956, 19: 452–467.

Cracco, R.Q. and Cracco, J.B. Somatosensory evoked potentials in man: far-field potentials. Electroenceph. clin. Neurophysiol., 1976, 41: 460–466.

Debecker, J. et Desmedt, J.E. Les potentiels évoqués cérébraux et les potentiels de nerf sensible chez l'homme. Acta neurol. belg., 1964, 64: 1212–1248.

Dejérine, J. et Thomas A. Contribution à l'étude du trajet intramédullaire des racines postérieures dans la région cervicale et dorsale supérieure de la moelle épinière. C.R. Soc. Biol. (Paris), 1896, 48: 675–679.

Desmedt, J.E. Somatosensory cerebral evoked potentials in man. In: A. Rémond (Ed.), Handbook of Electroencephalography and Clinical Neurophysiology, Vol. 9. Elsevier, Amsterdam, 1971: 55–82.

Desmedt, J.E. Some observations on the methodology of cerebral evoked potentials in man. In: J.E. Desmedt (Ed.), Attention, Voluntary Contraction and Event-Related Cerebral Potentials. Progr. clin. Neurophysiol., Vol. 1. Karger, Basel, 1977: 12–29.

Desmedt, J.E. Noninvasive analysis of the spinal cord generators activated by somatosensory input in man: nearfield and farfield components. Exp. Brain Res., 1984, Suppl. 19: 45–62.

Desmedt, J.E. and Bourguet, M. Colour imaging of parietal and frontal somatosensory potential fields evoked by stimulation of median or posterior tibial nerve in man. Electroenceph. clin. Neurophysiol, 1985, 62: 1–17.

Desmedt, J.E. and Cheron, G. Central somatosensory conduction in man: neural generators and interpeak latencies of the far-field components recorded from neck and right or left scalp and earlobes. Electroenceph. clin. Neurophysiol., 1980, 50: 382–403.

Desmedt, J.E. and Cheron, G. Prevertebral (oesophageal) recording of subcortical somatosensory evoked potentials in man: the spinal P13 component and the dual nature of the spinal generators. Electroenceph. clin. Neurophysiol., 1981a, 52: 257–275.

Desmedt, J.E. and Cheron, G. Non-cephalic reference recording of early somatosensory potentials to finger stimulation in adult or aging man: differentiation of widespread N18 and contralateral N20 from the prerolandic P22 and N30 components. Electroenceph. clin. Neurophysiol., 1981b, 52: 553–570.

Desmedt, J.E., Brunko, E., Debecker, J. and Carmeliet, J. The system bandpass required to avoid distortion of early components when averaging somatosensory evoked potentials. Electroenceph. clin. Neurophysiol., 1974, 37: 407–410.

Desmedt, J.E., Nguyen, T.H. and Carmeliet, J. Unexpected latency shifts of the stationary P9 somatosensory evoked potential far field with changes in shoulder position. Electroenceph. clin. Neurophysiol., 1983, 56: 628–634.

Donchin, E., Callaway, E., Cooper, R., Desmedt, J.E., Goff, W.R., Hillyard, S.A. and Sutton, S. Publication criteria for studies of evoked potentials in man. In: J.E. Desmedt (Ed.), Attention, Voluntary Contraction and Event-Related Cerebral Potentials. Progr. clin. Neurophysiol., Vol. 1. Karger, Basel, 1977: 1–11.

Duffy, F., Burchfiel, J.L. and Lombroso, C.T. Brain electrical activity mapping (BEAM): a method for extending the clinical utility of EEG and evoked potentials data. Ann. Neurol., 1978, 5: 309–321.

El Negamy, E. and Sedgwick, E.M. Properties of a spinal somatosensory evoked potential recorded in man. J. Neurol. Neurosurg. Psychiat., 1978, 41: 762–768.

Emerson, D.G., Seyal, M. and Pedley, T.A. Somatosensory evoked potentials following median nerve stimulation: the cervical components. Brain, 1984, 107: 169–182.

Estrin, T. and Uzgalis, R. Computerized display of spatio-temporal EEG patterns. Trans. biomed. Engng, 1969, BME-16: 192–196.

Ganes, T. and Nakstad, P. Subcomponents of the cervical evoked response in patients with intracerebral circulatory arrest. J. Neurol. Neurosurg. Psychiat., 1984, 47: 292–297.

Gasser, H.S. and Graham, H.T. Potentials produced in the spinal cord by stimulation of dorsal roots. Amer. J. Physiol., 1933, 103: 303–320.

Goff, W.R., Rosner, B.S. and Allison, T. Distribution of somatosensory evoked responses in normal man. Electroenceph. clin. Neurophysiol., 1962, 14: 697–713.

Halliday, A.M. and Wakefield, G.S. Cerebral evoked potentials in patients with dissociated sensory loss. J. Neurol. Neurosurg. Psychiat., 1963, 26: 211–219.

Hashimoto, I. Somatosensory evoked potentials from the human brain-stem: origins of short-latency potentials. Electro-

enceph. clin. Neurophysiol., 1984, 57: 221–227.
Hume, A.L. and Cant, B.R. Conduction time in central somatosensory pathways in man. Electroenceph. clin. Neurophysiol., 1978, 45: 361–375.
Hume, A.L. and Cant, B.R. Central somatosensory conduction after head injury. Ann. Neurol., 1981, 10: 411–419.
Jewett, D.L. and Williston, J.S. Auditory evoked far-fields averaged from the scalp in humans. Brain, 1971, 94: 681–696.
Jones, S.J. Short-latency potentials recorded from the neck and scalp following median nerve stimulation in man. Electroenceph. clin. Neurophysiol., 1977, 43: 853–863.
Kimura, J., Mitsudome, A., Beck, D.O., Yamada, T. and Dickins, Q.S. Field distribution of antidromically activated digital nerve potentials: model for far-field recording. Neurology (Minneap.), 1983, 33: 1164–1169.
Klee, M. and Rall, W. Computed potentials of cortically arranged populations of neurons. J. Neurophysiol., 1977, 40: 647–666.
Kritchevsky, M. and Wiederholt, W.C. Short-latency somatosensory evoked responses in man. Arch. Neurol. (Chic.), 1978, 35: 706–711.
Lehmann, D. and Skrandies, W. Reference-free identification of components of checkerboard-evoked multichannel potential fields. Electroenceph. clin. Neurophysiol., 1980, 48: 609–621.
Lesser, R.P., Lueders, H., Hahn, J. and Klem, G. Early somatosensory potentials evoked by median nerve stimulation: intraoperative monitoring. Neurology (Minneap.), 1981, 31: 1519–1523.
Lindblom, U.F. and Ottoson, J.O. Localization of the structure generating the negative cord dorsum potential evoked by stimulation of low-threshold cutaneous fibres. Acta physiol. scand., 1953, 29 (Suppl. 106): 180–190.
Lorente de Nó, R. A Study of Nerve Physiology. Studies from the Rockefeller Institute, New York, 1947.
Lueders, H., Lesser, R., Hahn, J., Little, J. and Klem, G. Subcortical somatosensory evoked potentials to median nerve stimulation. Brain, 1983, 106: 341–372.
Matthews, W.B., Beauchamp, M. and Small, D.G. Cervical somatosensory evoked responses in man. Nature (Lond.), 1974, 52: 230–232.
Mauguière, F., Courjon, J. and Schott, B. Dissociation of early SEP components in unilateral traumatic section of the lower medulla. Ann. Neurol., 1983a, 13: 309–313.
Mauguière, F., Desmedt, J.E. and Courjon, J. Neural generators of N18 and P14 far-field somatosensory evoked potentials: patients with lesion of thalamus or thalamo-cortical radiations. Electroenceph. clin. Neurophysiol., 1983b, 56: 283–292.
Nakanishi, T. Action potentials recorded by fluid electrodes. Electroenceph. clin. Neurophysiol., 1982, 53: 343–345.
Nakanishi, T., Shimada, Y., Sakuta, M. and Toyokura, Y. The initial positive component of scalp-recorded somatosensory evoked potentials in normal subjects and in patients with neurological disorders. Electroenceph. clin. Neurophysiol., 1978, 45: 26–34.
Nielson, K.L. Methods in Numerical Analysis. Macmillan, New York, 1956.
Noel, P. and Desmedt, J.E. Somatosensory cerebral evoked potentials after vascular lesions of the brainstem and diencephalon. Brain, 1975, 98: 113–128.
Pratt, H., Starr, A., Amlie, R.N. and Politoske, D. Mechanically and electrically evoked somatosensory potentials in normal humans. Neurology (Minneap.), 1979, 29: 1236–1244.
Ragot, R.A. and Rémond, A. EEG field mapping. Electroenceph. clin. Neurophysiol., 1978, 45: 417–421.
Rémond, A. et Lesèvre, N. Distribution topographique et potentiels évoqués visuels occipitaux chez l'homme normal. Rev. neurol., 1965, 112: 317–330.
Rethelyi, M. and Szentágothai, J. Distribution and connexions of afferent fibres in the spinal cord. In: A. Iggo (Ed.), Handbook of Sensory Physiology, Vol. 2. Springer, Berlin, 1973: 207–252.
Rexed, B. A cytoarchitectonic atlas of the spinal cord in the cat. J. comp. Neurol., 1954, 100: 297–379.
Shibasaki, H., Ohnishi, A. and Kuroiwa, Y. Use of SEPs to localize degeneration in a rare polyneuropathy: studies on polyneuropathy associated with pigmentation, hypertrichosis, edema and plasma cell dyscrasia. Ann. Neurol., 1982, 12: 355–360.
Small, D.G., Beauchamp, M. and Matthews, W.B. Subcortical somatosensory evoked potentials in normal man and patients with central nervous system lesions. In: J.E. Desmedt (Ed.), Uses of Cerebral, Brainstem and Spinal Somatosensory Evoked Potentials. Progr. clin. Neurophysiol., Vol. 7. Karger, Basel, 1980: 190–204.
Sprague, J.M. and Hong, C.H. The terminal fields of dorsal root fibers in the lumbosacral spinal cord of the cat, and the dendrite organization of the motor nuclei. Progr. Brain Res., 1964, 11: 120–154.
Stockard, J.J. and Sharbrough, F.W. Unique contributions of short-latency auditory and somatosensory evoked potentials to neurologic diagnosis. In: J.E. Desmedt (Ed.), Clinical Uses of Cerebral, Brainstem and Spinal Somatosensory Evoked Potentials. Progr. clin. Neurophysiol., Vol. 7. Karger, Basel, 1980: 231–263.
Symon, L., Hargadine, J., Zawirski, M. and Branston, N. Central conduction time as an index of ischaemia in subarachnoid haemorrhage. J. neurol. Sci., 1979, 44: 95–103.
Wall, P.D. The laminar organization of dorsal horn and effects of descending impulses. J. Physiol. (Lond.), 1967, 188: 403–423.
Walter, W.G. and Shipton, H.W. A new toposcopic display system. Electroenceph. clin. Neurophysiol., 1951, 3: 281–292.
Willis, W.D. and Coggeshall, R.E. Sensory Mechanisms of the Spinal Cord. Plenum Press, New York, 1978.
Yamada, T., Kimura, J. and Nitz, D.M. Short-latency somatosensory evoked potentials following median nerve stimulation in man. Electroenceph. clin. Neurophysiol., 1980, 48: 367–376.
Yamada, T., Kimura, J., Wilkinson, J.T. and Kayamori, R. Short- and long-latency median somatosensory evoked potentials. Arch. Neurol. (Chic.), 1983, 40: 215–220.